Wavelength-selective switching using double-ring resonators coupled by a three-waveguide directional coupler

Linjie Zhou,[1,*] Richard Soref,[2] and Jianping Chen[1]

[1]*State Key Laboratory of Advanced Optical Communication Systems and Networks Department of Electronic Engineering, Shanghai Jiao Tong University, Shanghai 200240, China*

[2]*The Engineering Program, University of Massachusetts at Boston, 100 Morrissey Blvd., Boston, Massachusetts 02125, USA*

[*]*ljzhou@sjtu.edu.cn*

Abstract: A novel design of a two-bus coupled-rings 2 × 2 switch with inter-ring coupling enabled by a three-waveguide (3w) directional coupler is proposed. The device is analyzed using a theoretical model based on coupled mode theory and optical transfer formulae. We show that injected free-carriers tuning of the central waveguide in the 3w coupler affects only the bonding resonance mode while the other anti-bonding mode is transparent. This feature can be used to perform selective optical switching, and a numerical design example is given on the silicon photonics platform. The selective switch can be employed in a two-color duplex bidirectional communication system which conveniently separates the simultaneous transmitted and received signals in a single fiber-optic waveguide.

OCIS codes: (230.5750) Resonators; (130.4815) Optical switching devices; (250.5300) Photonic integrated circuits; (230.3120) Integrated optics devices.

References and links

1. N. Farrington, G. Porter, S. Radhakrishnan, H. H. Bazzaz, V. Subramanya, Y. Fainman, G. Papen, and A. Vahdat, "Helios: a hybrid electrical/optical switch architecture for modular data centers," ACM SIGCOMM Comp. Comm. Rev. **41**, 339–350 (2011).
2. R. Tucker, "Green optical communications—Part II: Energy limitations in networks," IEEE J. Sel. Top. Quantum Electron. **17**(2), 261–274 (2011).
3. L. Lu, L. Zhou, Z. Li, X. Li, and J. Chen, "Broadband 4× 4 non-blocking silicon electro-optic switches based on Mach-Zehnder interferometers," IEEE Photon. J. **7**, 7800108 (2015).
4. L. Lu, L. Zhou, S. Li, Z. Li, X. Li, and J. Chen, "4× 4 non-blocking silicon thermo-optic switches based on multimode interferometers," J. Lightwave Technol. **33**(4), 857–864 (2015).
5. K. Tanizawa, K. Suzuki, M. Toyama, M. Ohtsuka, N. Yokoyama, K. Matsumaro, M. Seki, K. Koshino, T. Sugaya, and S. Suda, "32× 32 strictly non-blocking Si-wire optical switch on ultra-small die of 11× 25 mm^2," in *Optical Fiber Communication Conference*(Optical Society of America, 2015), p. M2B. 5.
6. X. Li, X. Xiao, H. Xu, Z. Li, T. Chu, J. Yu, and Y. Yu, "Mach-Zehnder-based five-port silicon router for optical interconnects," Opt. Lett. **38**(10), 1703–1705 (2013).
7. B. G. Lee, A. V. Rylyakov, W. M. Green, S. Assefa, C. W. Baks, R. Rimolo-Donadio, D. M. Kuchta, M. H. Khater, T. Barwicz, C. Reinholm, E. Kiewra, S. M. Shank, C. L. Schow, and Y. A. Vlasov, "Monolithic silicon integration of scaled photonic switch fabrics, CMOS logic, and device driver circuits," J. Lightwave Technol. **32**(4), 743–751 (2014).
8. L. Chen and Y. K. Chen, "Compact, low-loss and low-power 8×8 broadband silicon optical switch," Opt. Express **20**(17), 18977–18985 (2012).
9. P. Dong, S. Liao, H. Liang, R. Shafiiha, D. Feng, G. Li, X. Zheng, A. V. Krishnamoorthy, and M. Asghari, "Submilliwatt, ultrafast and broadband electro-optic silicon switches," Opt. Express **18**(24), 25225–25231 (2010).
10. L. Zhou, S. S. Djordjevic, R. Proietti, D. Ding, S. J. B. Yoo, R. Amirtharajah, and V. Akella, "Design and evaluation of an arbitration-free passive optical crossbar for on-chip interconnection networks," Appl. Phys., A Mater. Sci. Process. **95**(4), 1111–1118 (2009).
11. R. Ji, L. Yang, L. Zhang, Y. Tian, J. Ding, H. Chen, Y. Lu, P. Zhou, and W. Zhu, "Microring-resonator-based four-port optical router for photonic networks-on-chip," Opt. Express **19**(20), 18945–18955 (2011).

#237537 - $15.00 USD Received 3 Apr 2015; revised 6 May 2015; accepted 9 May 2015; published 13 May 2015

12. Y. Zhang, Y. Li, S. Feng, and A. W. Poon, "Towards adaptively tuned silicon microring resonators for optical networks-on-chip applications," IEEE J. Sel. Top. Quantum Electron. **20**(4), 136–149 (2014).
13. P. DasMahapatra, R. P. Stabile, A. A. Rohit, and K. A. Williams, "Optical crosspoint matrix using broadband resonant switches," IEEE J. Sel. Top. Quantum Electron. **20**(4), 1–10 (2014).
14. H. L. R. Lira, S. Manipatruni, and M. Lipson, "Broadband hitless silicon electro-optic switch for on-chip optical networks," Opt. Express **17**(25), 22271–22280 (2009).
15. X. Zhu, Q. Li, J. Chan, A. Ahsan, H. L. Lira, M. Lipson, and K. Bergman, "4x44 Gb/s packet-level switching in a second-order microring switch," IEEE Photon. Technol. Lett. **24**(17), 1555–1557 (2012).
16. L. Lu, L. Zhou, X. Li, and J. Chen, "Low-power 2×2 silicon electro-optic switches based on double-ring assisted Mach-Zehnder interferometers," Opt. Lett. **39**(6), 1633–1636 (2014).
17. L. Zhou and A. W. Poon, "Electrically reconfigurable silicon microring resonator-based filter with waveguide-coupled feedback," Opt. Express **15**(15), 9194–9204 (2007).
18. L. Zhou and A. W. Poon, "Fano resonance-based electrically reconfigurable add-drop filters in silicon microring resonator-coupled Mach-Zehnder interferometers," Opt. Lett. **32**(7), 781–783 (2007).
19. S. Darmawan, Y. M. Landobasa, and M. K. Chin, "Nested ring Mach-Zehnder interferometer," Opt. Express **15**(2), 437–448 (2007).
20. S.-Y. Cho and R. Soref, "Interferometric microring-resonant 2 x 2 optical switches," Opt. Express **16**(17), 13304–13314 (2008).
21. Y. Chen, S.-T. Ho, and V. Krishnamurthy, "All-optical switching in a symmetric three-waveguide coupler with phase-mismatched absorptive central waveguide," Appl. Opt. **52**(36), 8845–8853 (2013).
22. R. Soref, "Mid-infrared 2× 2 electro-optical switching by silicon and germanium three-waveguide and four-waveguide directional couplers using free-carrier injection," Photon. Res. **2**(5), 102–110 (2014).
23. D. G. Rabus, *Integrated Ring Resonators* (Springer, 2007).
24. Z. Lu, H. Yun, Y. Wang, Z. Chen, F. Zhang, N. A. F. Jaeger, and L. Chrostowski, "Broadband silicon photonic directional coupler using asymmetric-waveguide based phase control," Opt. Express **23**(3), 3795–3808 (2015).
25. M. Nedeljkovic, R. Soref, and G. Z. Mashanovich, "Free-carrier electrorefraction and electroabsorption modulation predictions for silicon over the 1–14-infrared wavelength range," IEEE Photon. J. **3**(6), 1171–1180 (2011).
26. A. H. Atabaki, A. A. Eftekhar, M. Askari, and A. Adibi, "Accurate post-fabrication trimming of ultra-compact resonators on silicon," Opt. Express **21**(12), 14139–14145 (2013).
27. L. Zhou, K. Okamoto, and S. J. B. Yoo, "Athermalizing and trimming of slotted silicon microring resonators with UV-sensitive PMMA upper-cladding," IEEE Photon. Technol. Lett. **21**(17), 1175–1177 (2009).
28. L. Zhou, X. Zhang, L. Lu, and J. Chen, "Tunable vernier microring optical filters with p-i-p type microheaters," IEEE Photon. J. **5**, 6601211 (2013).
29. X. Xiao, X. Li, H. Xu, Y. Hu, K. Xiong, Z. Li, T. Chu, J. Yu, and Y. Yu, "44-Gb/s silicon microring modulators based on zigzag PN junctions," IEEE Photon. Technol. Lett. **24**(19), 1712–1714 (2012).

1. Introduction

Optical switches are basic components for optical signal routing for long-haul telecommunications and short-reach inter/intra-chip interconnects [1, 2]. They should be capable of processing ever-increasing data traffic with low power consumption and low latency. One approach is to use optical-electrical-optical (O-E-O) conversion with signal switching implemented in the electrical domain. Although that can utilize the mature electrical processing capability, the intrinsic speed limitation and power consumption of transceivers are the bottleneck to the large bandwidth requirement for optical transmission. Switching in the optical domain is a promising alternative as it provides transparent optical channels with their routing directions monitored and steered by control signals. Such switching can be realized by introducing a refractive index change based on electro-optic, thermo-optic, opto-mechanical, or nonlinear all-optical effects.

Mach-Zehnder interferometers (MZI) and ring resonators are widely used as the basic optical switching structures [3–13]. The free-carrier electrorefraction effect in Si or Ge is often applied to both of the above switches. It can provide nanosecond reconfiguration time, orders of magnitude faster than the thermo-optic and opto-mechanical effects (on the order of micron-seconds). The MZI is an interference device with its switching state flipped by inducing a π phase shift in one arm with respect to the other. Its spectral bandwidth is determined by the splitter and combiner, which usually cover 10's of nm. As the refractive index change is always accompanied by some small free-carrier absorption when using the free-carrier electrorefraction effect, power switching is not complete at the bar-state, leading to increased insertion loss and crosstalk. Moreover, large power consumption is required to

#237537 - $15.00 USD Received 3 Apr 2015; revised 6 May 2015; accepted 9 May 2015; published 13 May 2015

achieve the π-phase shift needed for switching. An efficient solution to reduce the power consumption is to use a longer modulation arm as demonstrated in [9]. The ring resonator is a more compact structure, and only a small phase change of $2\pi/f$ (f is the resonance finesse) induced around the ring waveguide circumference is enough to shift one resonance linewidth. Hence, the required phase shift can be much smaller than for the MZI structure if a high quality factor (Q-factor) and small-size resonator is used. As light does not go through the resonator at the bar state with voltage on, free-carrier electroabsorption is less deleterious there than in the MZI. The disadvantage of the ring resonator switch is that its spectral bandwidth is λ/Q, inversely proportional to the Q-factor.

A single ring resonator has a Lorentzian resonance lineshape, with the slow and long tail being a limiting factor to achieve high switching extinction ratio and low crosstalk in 2 × 2 ring switches. Second-order double-ring-based switches have been demonstrated to have a faster roll-off, which can provide lower crosstalk than the single ring switch [14, 15]. The MZI and ring resonator can also be combined in side-coupled or nested configurations to make use of both merits to improve the switching performance [16–20]. We have previously demonstrated that a short MZI coupled with a ring resonator in each arm can have low crosstalk and low power switching operation [16].

Recently, directional couplers composed of three parallel waveguides as optical switches were proposed and studied [21, 22]. It was shown that optical switching can be realized by changing the complex refractive index of the central waveguide. Light coupling to the side waveguides is controlled by both the phase change and loss increment of the central waveguide, leading to rather complete crossbar broad-spectrum switching. Using four-waveguide directional couplers can reduce the coupling length by a half compared to the three-waveguide switch [22]. The directional couplers in Si or Ge need to work in the weak coupling regime so that the required refractive index change can be accomplished by injection of a reasonable concentration of electrons and holes, which inevitably makes the device long.

Here we propose an optical switch based on two racetrack ring resonators coupled through a three-waveguide (3w) directional coupler. The refractive index tuning is performed to the central waveguide of the 3w coupler working in the full coupling condition. We find that the coupled resonators possess two resonance modes with distinct responses to the index tuning: one resonance mode can be shifted while the other is always locked in spectrum. This novel switch can be applied in a one-fiber bidirectional transmission system to simultaneously gate transmission and receipt of wavelength division multiplexed (WDM) optical signals.

2. Device structure and modeling

Figure 1(a) shows our proposed device structure consisting of two racetrack ring resonators. The two rings are coupled through a 3w directional coupler, and coupled with two parallel bus waveguides through two-waveguide (2w) directional couplers. The structure is similar to a well-known two-ring add-drop filter (ADF) except that it has an additional output port (denoted as the 'idle' port). Neither ring is disturbed here, so they are both passive. Instead, tuning is performed to the 3w coupler with the refractive index of its central waveguide adjustable. The length of the 2w and 3w couplers is L_c.

To analyze the device, we first employ coupled mode theory to model the 2w and 3w couplers. The coupling between the straight waveguide and the bending part of the ring waveguide is neglected for simplicity of modeling yet it will not affect the general conclusions of our analyses. The normalized complex field transmission coefficient a_1 and coupling coefficient a_2 of the 2w coupler is given by [21]:

$$a_1 = A_1 e^{i\phi_{2w}} = \cos\left(\kappa_{2w} L_c\right) e^{i\beta_1 L_c} \tag{1}$$

$$a_2 = A_2 e^{i\phi_{2w}} = i\sin\left(\kappa_{2w} L_c\right) e^{i\beta_1 L_c} \tag{2}$$

#237537 - $15.00 USD Received 3 Apr 2015; revised 6 May 2015; accepted 9 May 2015; published 13 May 2015

where $A_{1,2}$ is the amplitude of $a_{1,2}$, β_1 is the propagation constant of the bus and ring waveguides and κ_{2w} is the coupling coefficient of the 2w coupler. The coupled power is $|a_1|^2$ and $|a_2|^2$ and power conservation is satisfied for a lossless coupler ($|a_1|^2 + |a_2|^2 = 1$). The coupling strength is determined by $\kappa_{2w}L_c$, and full coupling is achieved when $L_c = \pi/2\,\kappa_{2w}$.

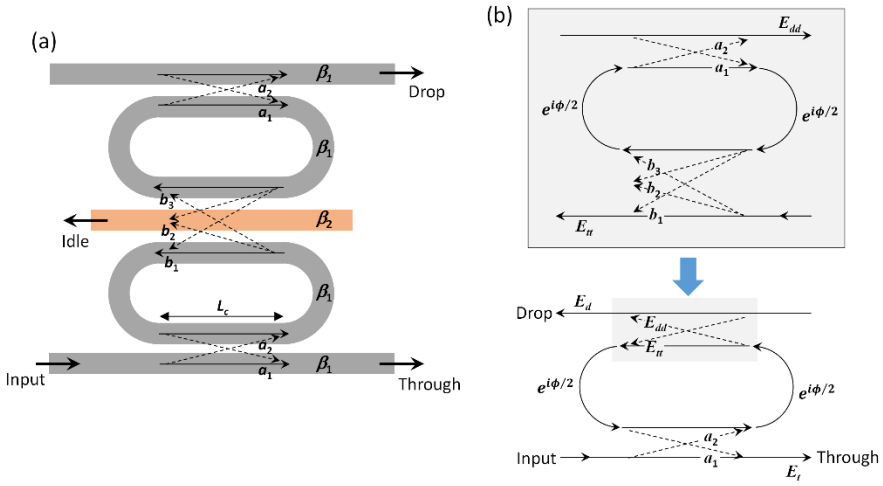

Fig. 1. (a) Schematic structure of the double-racetrack ring switch constructed by 2w and 3w couplers. (b) Transfer matrix modeling of the device using a recursive fashion.

Next we consider the 3w coupler which enables the inter-ring coupling. The first and third waveguides composing the racetrack ring resonators are identical with a propagation constant of β_1 and the central waveguide has a propagation constant of $\beta_2 = \beta_1 + \Delta\beta$. The phase change of the active waveguide is hence $\Delta\beta L_c$. For silicon waveguides, the refractive index change can be induced by the thermo-optic effect or the free-carrier plasma dispersion effect. For the latter effect, waveguide loss is also increased upon tuning, which is manifested by the complex propagation constant $\beta_2 = \beta_{2r} + i\alpha$ with the real and imaginary parts governed by the electrorefraction and electroabsorption effects respectively. Assuming the active waveguide is side-coupled to the two passive waveguides with a coupling coefficient of κ_{3w}, we can derive from the coupled mode equations the complex field transmission and coupling coefficients of the 3w coupler as (light is launched from the first waveguide) [21]:

$$b_1 = B_1 e^{i\beta_{ave}L_c} = \left[\frac{1}{2}\left(\cos\gamma_{3w}L_c - i\frac{\Delta_{3w}}{\gamma_{3w}}\sin\gamma_{3w}L_c + e^{-i\Delta_{3w}L_c}\right)\right]e^{i\beta_{ave}L_c} \tag{3}$$

$$b_2 = B_2 e^{i\beta_{ave}L_c} = \left(i\frac{\kappa_{3w}}{\gamma_{3w}}\sin\gamma_{3w}L_c\right)e^{i\beta_{ave}L_c} \tag{4}$$

$$b_3 = B_3 e^{i\beta_{ave}L_c} = \left[\frac{1}{2}\left(\cos\gamma_{3w}L_c - i\frac{\Delta_{3w}}{\gamma_{3w}}\sin\gamma_{3w}L_c - e^{-i\Delta_{3w}L_c}\right)\right]e^{i\beta_{ave}L_c} \tag{5}$$

where $B_{1,2,3}$ is the amplitude of $b_{1,2,3}$ and

$$\Delta_{3w} = \frac{\Delta\beta}{2} = \frac{\beta_2 - \beta_1}{2} \tag{6}$$

#237537 - $15.00 USD Received 3 Apr 2015; revised 6 May 2015; accepted 9 May 2015; published 13 May 2015

$$\beta_{ave} = \frac{\beta_1 + \beta_2}{2} \tag{7}$$

$$\gamma_{3w} = \sqrt{\Delta_{3w}^2 + 2\kappa_{3w}^2} \tag{8}$$

At the zero-injection off-state (voltage turned off), $\Delta\beta = 0$ and complete crossover from the first waveguide to the third waveguide is achieved when $L_c = \pi/\sqrt{2}\,\kappa_{3w}$.

For the coupled ring resonators, the normalized field at the through and drop ports can be expressed in a recursive fashion using the optical field transfer matrix method [23]. The upper part of the device (including the upper 2w coupler, the upper ring resonator and the 3w coupler) can be regarded as a complex coupler with the transmission and coupling coefficients being E_{tt} and E_{dd}, respectively, as shown in Fig. 1(b). Then, the whole device becomes a single ring ADF and the electric field at the through port can be expressed as

$$E_t = \frac{a_1 - (a_1^2 - a_2^2)E_{tt}e^{i\phi}}{1 - a_1 E_{tt} e^{i\phi}} \tag{9}$$

where $\phi = (2\pi R)\beta_1$ is the phase of the circular waveguide in racetrack ring resonators and R is the bending radius. E_{tt} is the through transmission of the upper ring ADF given by

$$E_{tt} = \frac{b_1 - (b_1^2 - b_3^2)a_1 e^{i\phi}}{1 - b_1 a_1 e^{i\phi}} \tag{10}$$

The transmission intensity is the squared amplitude of electric field

$$I_t = |E_t|^2 = \left| \frac{1}{A_1} \frac{\left(e^{i\Phi} - z_1\right)\left(e^{i\Phi} - z_2\right)}{\left(e^{i\Phi} - p_1\right)\left(e^{i\Phi} - p_2\right)} \right|^2 \tag{11}$$

where the zeros and poles are given by

$$z_1 = \frac{A_1^2 B_1 + B_1 + \sqrt{A_2^4 B_1^2 + 4A_1^2 B_3^2}}{2A_1\left(B_1^2 - B_3^2\right)} \tag{12}$$

$$z_2 = \frac{A_1^2 B_1 + B_1 - \sqrt{A_2^4 B_1^2 + 4A_1^2 B_3^2}}{2A_1\left(B_1^2 - B_3^2\right)} \tag{13}$$

$$p_1 = \frac{1}{A_1\left(B_1 - B_3\right)} = \frac{1}{\cos\left(\kappa_{2w} L_c\right)} e^{i\Delta_{3w} L_c} \tag{14}$$

$$p_2 = \frac{1}{A_1\left(B_1 + B_3\right)} = \frac{1}{\cos\left(\kappa_{2w} L_c\right)\left[\cos\left(\gamma_{3w} L_c\right) - i\frac{\Delta_{3w}}{\gamma_{3w}}\sin\left(\gamma_{3w} L_c\right)\right]} \tag{15}$$

And $\Phi = \Phi_0 + \Delta\Phi = \left(\phi + 2\beta_1 L_c\right) + \Delta\beta L_c/2$ consisting of a fixed ring round trip phase (Φ_0) and a phase change in the active waveguide ($\Delta\beta L_c$).

The field at the drop port can also be expressed as

$$E_d = \frac{a_2 E_{dd} e^{i\phi/2}}{1 - a_1 E_{tt} e^{i\phi}} \tag{16}$$

#237537 - $15.00 USD Received 3 Apr 2015; revised 6 May 2015; accepted 9 May 2015; published 13 May 2015

where E_{dd} is the drop transmission of the upper ring ADF given by

$$E_{dd} = \frac{a_2 b_3 e^{i\phi/2}}{1 - a_1 b_1 e^{i\phi}} \tag{17}$$

The output intensity at the drop port is

$$I_d = \left|E_d\right|^2 = \left| A_2^2 B_3 \frac{p_1}{e^{i\Phi} - p_1} \frac{p_2}{e^{i\Phi} - p_2} \right|^2 \tag{18}$$

The field at the idle port is the summation of out-coupled fields from the two racetrack ring resonators and hence is expressed as

$$E_i = \frac{a_1 b_2 E_{dd} e^{i\phi}}{1 - a_1 E_{tt} e^{i\phi}} + \frac{a_2 b_2 e^{i\phi/2}}{1 - a_1 E_{tt} e^{i\phi}} \tag{19}$$

and the output intensity is

$$I_i = \left|E_i\right|^2 = \left| A_2 B_2 \frac{p_2}{e^{i\Phi} - p_2} \right|^2 \tag{20}$$

Equations (11), (18) and (20) determine the transmission spectra at the three output ports of the device.

3. Characteristics of resonances

We first consider the off-state ($\Delta\beta = 0$) where the 3w coupler works at the complete crossover state, and we have $\gamma_{3w} L_c = \pi$. The two poles are reduced to

$$p_1\left(\Delta\beta = 0\right) = \frac{1}{\cos\left(\kappa_{2w} L_c\right)} \tag{21}$$

$$p_2\left(\Delta\beta = 0\right) = -\frac{1}{\cos\left(\kappa_{2w} L_c\right)} \tag{22}$$

It is notable that the two poles differ by a π phase, implying the two sets of resonances are equally spaced in the spectrum.

We next consider the carrier-injected voltage-on state where the active waveguide in the 3w waveguide is perturbed with an increased propagation constant $\Delta\beta$. According to (11) and (18), resonance occurs when the total round-trip phase Φ is equal to the phase of the pole p_1 or p_2. For the first resonance (mode A), assuming $\kappa_{2w} L_c < \pi/2$, the phase of p_1 becomes $\Delta_{3w} L_c$. Thus, the resonance condition would be $\Phi = \Delta_{3w} L_c + 2m\pi$, leading to $\Phi_0 = 2m\pi$. It suggests this resonance is locked in the spectrum and cannot be tuned by the 3w coupler. For the second resonance (mode B), the phase of p_2 is locked to π under the assumption of small perturbation which satisfies $\Delta_{3w} \ll \kappa_{3w}$. Thus the resonance condition would be $\Phi = \pi + 2m\pi$, leading to $\Phi_0 = (2m + 1)\pi - \Delta\beta L_c/2$. It indicates that this wavelength channel can be effectively tuned by the 3w coupler. Figure 2 shows the shift of the two resonances versus phase tuning ($\Delta\beta L_c$). It can be seen that only mode B can effectively respond to $\Delta\beta L_c$. The resonance of mode B shifts linearly $\Delta\beta L_c$ when it is small. The change slope that determines the tuning efficiency is $0.25\mathrm{FSR}/\pi$, with FSR being the free spectral range of resonances. The largest tuning range while maintaining a good tuning efficiency is approximately 1.5π, after which the resonance shift becomes flat when the small Δ_{3w} assumption fails.

#237537 - $15.00 USD Received 3 Apr 2015; revised 6 May 2015; accepted 9 May 2015; published 13 May 2015

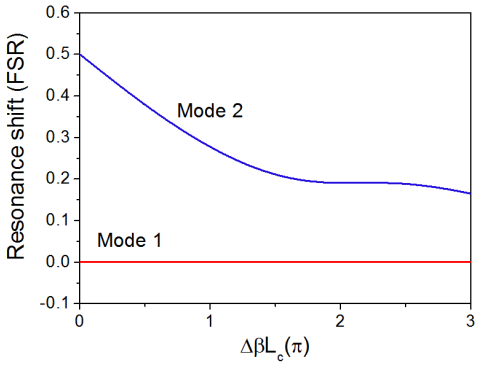

Fig. 2. Resonance shift versus $\Delta\beta L_c$ for the two resonance modes.

We next calculate the transmission spectrum of the switch. The coupling coefficients for the 2w and 3w couplers are chosen to be $\kappa_{2w} = 0.02$ μm^{-1} and $\kappa_{3w} = 0.1$ μm^{-1}, respectively. To satisfy the complete crossover for the 3w coupler ($B_1 = B_2 = 0$, $B_3 = 1$), the 3w coupler needs to be operated at one full coupling length of $L_c = \sqrt{2}\pi/2\kappa_{3w}$. Figure 3 shows the transmission spectra of the through and drop ports when $\Delta\beta L_c$ varies from 0 to π. Resonance mode B shifts to approach mode A while mode A is totally frozen. Therefore, only an alternative channel is switchable by the active 3w coupler. Equation (20) reveals that only one pole p_2 is present in the idle transmission function, acting as an optical leakage channel for mode B. The leakage grows upon tuning of the 3w coupler. The leakage is high only when the 3w coupler deviates significantly from the complete crossover condition. For example, the leakage at the idle port increases to 0.46 when $\Delta\beta L_c = \pi$, where the crossover coupling is reduced to $B_3 = 0.74$.

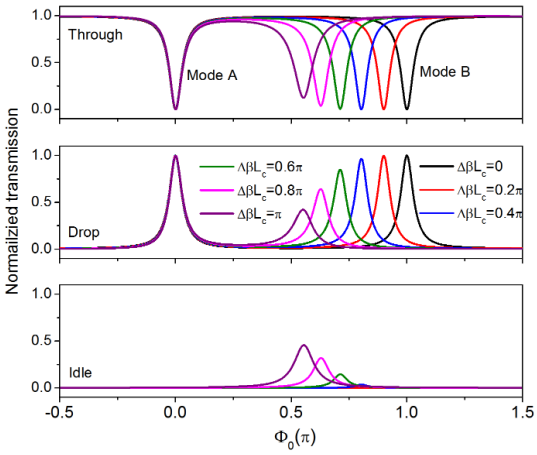

Fig. 3. Transmission spectra of the three output ports changing as a function of $\Delta\beta L_c$.

4. Numerical example

We next consider the device implementation based on submicron-size silicon waveguides. The waveguide effective refractive index is assumed to be 2.52 which is a typical value for silicon-on-insulator (SOI) sub-micrometer strip waveguides. The coupling coefficient for the 2w and 3w couplers are chosen to be $\kappa_{2w} = 0.01$ μm^{-1} and $\kappa_{3w} = 0.07$ μm^{-1}, respectively. It should be noted that in general the coupling coefficients are sensitive to wavelength. Deviation of κ_{3w} from the designed value will give rise to increased crosstalk between the through and drop ports and more power leakage to the idle port, which will thus limit the

#237537 - $15.00 USD Received 3 Apr 2015; revised 6 May 2015; accepted 9 May 2015; published 13 May 2015

number of WDM channels available. Here, we choose fixed values of κ_{2w} and κ_{3w} in order to simply our calculation yet without losing generality. In fact, tricks could be played on the design of directional couplers to alleviate the wavelength dependence of coupling coefficients. For example, an asymmetric waveguide-based phase control section could be inserted in the directional coupler to compensate for the wavelength-dependent coupling ratios of the symmetric coupling sections [24]. The coupling strength can be controlled by choosing a proper gap separation between two waveguides in practical design. The coupling length is calculated to be L_c = 31.7 μm to satisfy the complete crossover condition for the 3w coupler. The ring radius is chosen to be 3 μm, which is large enough for the ring to incur negligible bending radiation loss.

The top panel in Fig. 4(a) shows the calculated transmission spectra of the through and drop ports. Periodic resonances with a 3-dB passband width of ~0.2 nm (25 GHz) are observable. As the complete crossover condition is satisfied for the 3w coupler, there is no power leakage to the idle port. In practice, there could be certain deviations from the ideal design due to various fabrication errors or when the wavelength is away from the targeted wavelength. The bottom panel in Fig. 4(a) shows the spectra when κ_{3w} is deviated by 5%. It can be seen that only mode B is affected with some power dropped to the idle port. To more clearly illustrate the influence of κ_{3w} on mode B, we plot the on-resonance transmitted power at 1542.34 nm from the three ports changing as a function of κ_{3w} in Fig. 4(b). The κ_{3w} needs to be controlled within 0.0677 μm^{-1} to 0.0723 μm^{-1} in order to get >20 dB power extinction ratio between through and drop ports. Such a device parameter can be obtained by using the state-of-the-art fabrication tools, which can control the waveguide width and gap variation within ~10 nm.

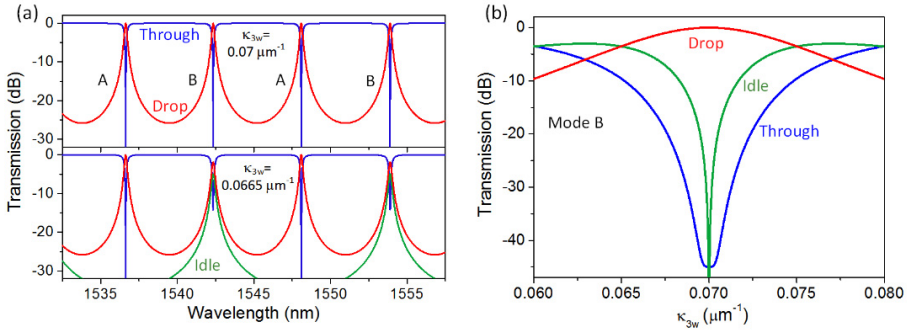

Fig. 4. (a) Calculated transmission spectra for two set of κ_{3w}. (c) On-resonance power transmission of the three ports as a function of κ_{3w} for mode B.

The 3w coupler tuning can be realized by free-carriers injection to the central waveguide. Due to the free-carrier ER and EA effects, the real and imaginary parts of the refractive index of silicon are changed [21], leading to phase shift and absorption loss. When free carriers are injected, only the resonances from mode B are blue-shifted while those from mode A are fixed. A carrier concentration of $\Delta N = \Delta P$ = 1e18 cm^{-3} can induce a blueshift of 0.32 nm [25], which flips the switching state if operating at the original resonance wavelengths as shown in Fig. 5(a). Note that the free-carrier absorption loss attenuates the shifted drop peak, which essentially improves the switching extinction ratio. The switching behavior can be clearly seen from the optical transmission variation in Fig. 5(b). The wavelength is fixed at the mode B resonance wavelength (1542.34 nm). The optical transmission is switched from the drop port to the through port when free carrier concentration increases. The bar-state insertion loss is 0.6 dB and the crosstalk is –10 dB with an injection concentration of 9e17 cm^{-3}. The insertion loss decreases to 0.1 dB and the crosstalk is –20 dB with an increased concentration of 3.3e18 cm^{-3}. It should be noted that the injection level can be reduced for a narrower

#237537 - $15.00 USD Received 3 Apr 2015; revised 6 May 2015; accepted 9 May 2015; published 13 May 2015

optical passband. In fact, there is a tradeoff between the channel bandwidth and the channel spacing under a certain injection level. A broader channel bandwidth means a lower resonance Q-factor, which inevitably leads to a slower roll-off. In order to maintain a certain crosstalk level for the bar state with voltage on, a larger resonance shift is needed. With a fixed injection level (thus fixed $\Delta\beta L_c$), this could only be obtained by increasing the channel spacing.

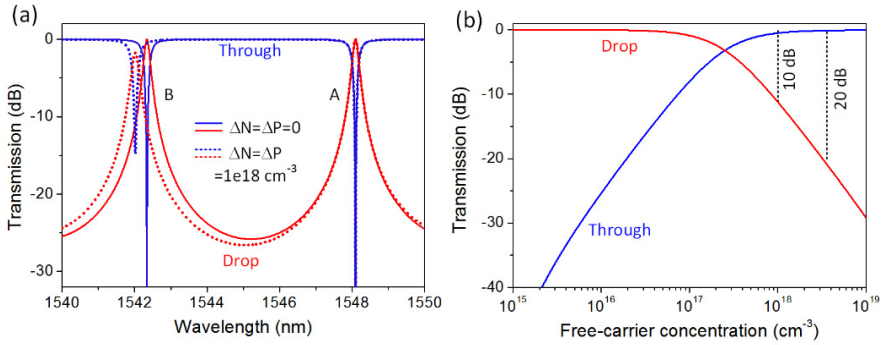

Fig. 5. (a) Transmission spectra of the through and drop ports before and after tuning. Free-carrier concentration increases to 1e18 cm^{-3} after voltage is turned on. (b) Optical power switching for mode B upon increment of free-carrier concentration.

To further study the origin of the distinct behavior of the two resonance modes, we use the two-dimensional finite-difference time-domain (FDTD) method to simulate the device. The simulated device has a smaller size than the above example to reduce computation memory and duration. Figure 6 shows the simulated steady-state optical field (H_z component) and optical power distributions in the device for the two modes. It is apparent that the major difference between the two modes lies in the 3w coupler. The optical power in mode A is located in the side waveguides with almost no power coupled to the central active waveguide. In contrast, the optical power in mode B is enhanced in the central waveguide, with even higher magnitude than in the ring waveguides. A close look at the field distribution reveals that the H_z field in mode A is anti-symmetric with respect to the central waveguide. On the contrary, the H_z field is symmetric in mode B. Therefore, we can regard the mode A as the anti-bonding mode while mode B is the bonding mode. The interaction of resonant optical field with free carriers determines the tuning efficiency of resonances. Therefore, it can be understood that mode A is immune to refractive index tuning owing to the absence of optical field in the active waveguide, and mode B is sensitive to tuning because of the enhanced optical field.

#237537 - $15.00 USD Received 3 Apr 2015; revised 6 May 2015; accepted 9 May 2015; published 13 May 2015

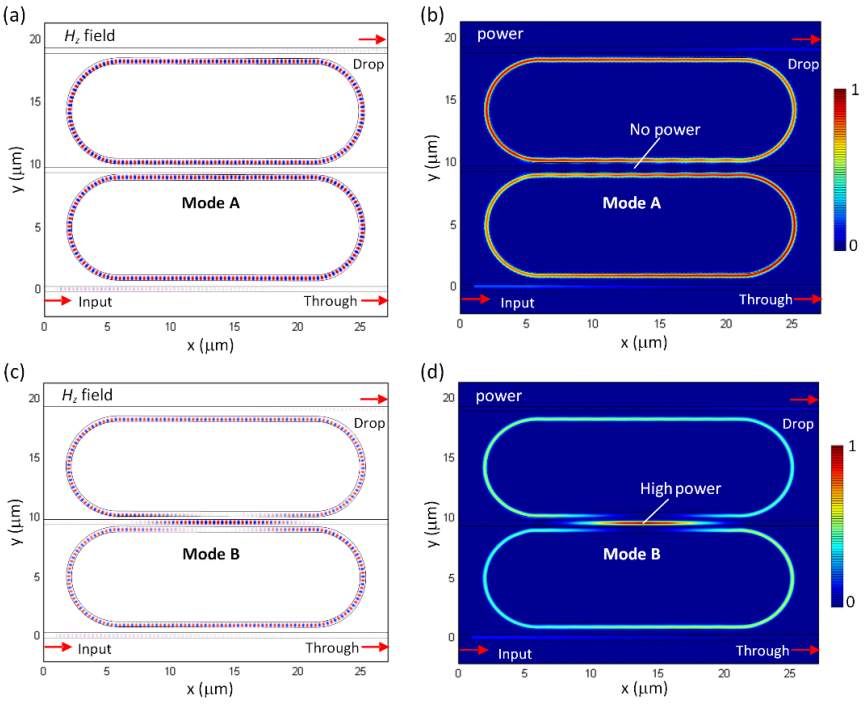

Fig. 6. FDTD simulation of the double-ring switch for (a) H_z-field of mode A, (b) optical power profile of mode A, (c) H_z-field of mode B, and (d) optical power profile of mode B.

5. Application to communication systems

We can use our device to construct a two-chip duplex communication system as shown in Fig. 7. The left ring switch has fixed resonance wavelengths at λ_i (i = 1, 3, …) and switchable wavelengths at λ_j (j = 2, 4, …). The left-end-of-link ring switch is connected to a transmitter (Tx_1) and a receiver (Rx_1) in such a way that the signal transmission at λ_j is gated by the voltage V_1 while incoming signals at λ_i are dropped to the receiver. In other words, the switch is operating on the transmitter but transparent to the receiver. The right end of the optical link is similar to the left end except that the ring resonances at right are shifted by a half FSR so that λ_i is switchable and λ_j fixed. The resonance shift in practice can be accomplished by careful design of the ring resonators. The size difference between left end and right end double-ring devices only causes a slight change in FSR. In our numerical example depicted in section 4, the wavelength spacing difference between the two modes is 0.022 nm which is almost one order smaller than the passband. Therefore, it is possible to simultaneously align the two resonance modes with a small number of channels. Wavelength fine tuning methods such as post-fabrication trimming [26, 27] and thermal optical tuning [28] can also be adopted to accurately align the resonance wavelengths. With this configuration, the incoming signal at λ_j is always routed to the local receiver (Rx_2) and the transmitted signal from the transmitter (Tx_2) is gated by the control voltage V_2. In this bidirectional transmission system, the WDM signals all go in one optical fiber (or bus optical waveguide) and our two-ring switch integrates both filtering and gating functions simultaneously, leading to a more compact system.

If a high speed microwave signal is applied instead of the DC control signal, the ring switch becomes a unidirectional modulator. The unmodulated light is absorbed in the attenuator at each end. The continuous wave light at λ_j from Tx_1 is modulated by the ring resonators before being transmitted to the fiber link. However, the incoming signal at λ_i from right-end Tx_2 modulated by V_2 is not affected by the V_1 microwave signal driving the left-end

#237537 - $15.00 USD Received 3 Apr 2015; revised 6 May 2015; accepted 9 May 2015; published 13 May 2015

ring device, providing a transparent receiving channel. And so, simultaneous wavelength-multiplexed duplex communication is enabled. To realize high speed modulation, forward-bias *p-i-n* diodes or reverse-bias *p-n* diodes can be integrated in the active waveguide. As seen from Fig. 7, modulation of the 3w coupler is essentially to modulate the ring resonance. Similar to a regular ring modulator, the modulation speed is limited by both the free-carriers dynamics and the photon lifetime in the resonator. Given that >40 Gb/s modulation speed has been demonstrated in ring modulators [29], it is possible to achieve the same level of modulation speed using our device. The dynamic extinction ratio upon modulation is determined by the magnitude of microwave signal as well as the electro-optic (EO) bandwidth of the modulator. It is worth mentioning that there is high isolation between transmitter and receiver at the same end due to the travelling-wave nature of the resonances in the ideal case. In practice, waveguide imperfections (e.g., sidewall roughness or defect) may induce back scattering, which as a result cause back reflection of the transmitted signal to the receiver, leading to intra-chip crosstalk.

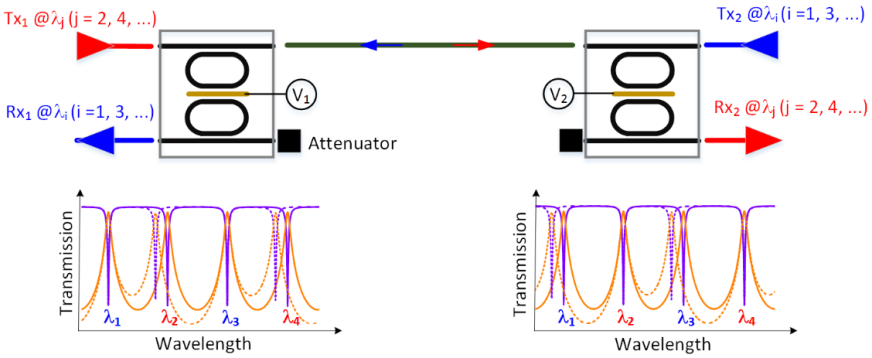

Fig. 7. Duplex bidirectional communication system using our ring switches.

6. Conclusion

We have proposed an optical switch made of two passive racetrack ring resonators coupled at middle through an active 3w directional coupler. Coupled mode theory and optical transfer formulae are employed to establish the theoretical model. It is shown that two resonance modes are present in the device which respond distinctly to refractive index tuning in the central waveguide of the 3w coupler. Mode A is always locked while mode B is tunable allowing for selective optical switching operation. A design example is given using silicon strip waveguides. The bar-state voltage-on insertion loss is 0.1 dB and the crosstalk is −20 dB at a carrier injection concentration of 3.3e18 cm^{-3}. FDTD simulation further reveals that the two modes have distinct optical power distribution in the 3w coupler, corresponding to anti-bonding and bonding resonances. Based on the unique selective resonant switching of our device, we propose a one-fiber simultaneous duplex bidirectional communication system which fully utilizes the selective switching/modulation capability of our device to separate transmission and reception of optical signals.

Acknowledgment

This work was supported in part by the 973 program (2011CB301700), the 863 program (2013AA014402), the National Natural Science Foundation of China (NSFC) (61422508), Science and Technology Commission of Shanghai Municipality (STCSM) Project (14QA1402600). R. Soref appreciates the support of the Air Force Office of Scientific Research (FA9550-14-1-0196) and the UK EPSRC on Project Migration.

#237537 - $15.00 USD Received 3 Apr 2015; revised 6 May 2015; accepted 9 May 2015; published 13 May 2015